ThermoTargetMiner as a proteome integral solubility alteration target database for prospective drugs against lung cancer

Hezheng Lyu[1,2], Hassan Gharibi[1,3], Bohdana Sokolova[1], Anna Voiland[4], Brady Nilsson[5], Zhaowei Meng[1,3,6], Massimiliano Gaetani[1,3,6], Amir Ata Saei[7*], Roman A. Zubarev[1,3,6,8,9*]

[1]Division of Physiological Chemistry I, Department of Medical Biochemistry and Biophysics, Karolinska Institutet, 171 65 Stockholm, Sweden

[2]Biomotif AB, 183 48 Täby, Sweden

[3]Chemical Proteomics, Swedish National Infrastructure for Biological Mass Spectrometry (BioMS), Stockholm, Sweden

[4]The French National Institute for Industrial Environment and Risks (Ineris), 60550 Verneuil-en-Halatte, France

[5]R&D, Fujifilm Irvine Scientific, 92705, USA

[6]SciLifeLab, Stockholm 171 77, Sweden

[7]Department of Microbiology, Tumor and Cell Biology, Karolinska Institutet, 171 65 Stockholm, Sweden

[8]Peoples Friendship University of Russia (RUDN University), 8 Miklukho-Maklaya St., Moscow, 117198 Russia

[9]The National Medical Research Center for Endocrinology, 115478 Moscow, Russia

*Correspondence and requests for materials should be addressed to A.A.S. (email: Amir.saei@ki.se) and R.A.Z. (email: Roman.Zubarev@ki.se)

Abstract

Knowledge of the targets of therapeutic compounds is vital for understanding their action mechanisms and side effects, but such valuable data is seldom available. The multiple complementary techniques needed for comprehensive target characterization must combine data reliability with sufficient analysis throughput. Here, we leveraged the Proteome Integral Solubility Alteration (PISA) assay to comprehensively characterize the targets of 67 approved drugs and candidate compounds against lung cancer. The analysis was performed on two cell lines representing different lung cancer phenotypes and novel targets for 77% of the tested molecules were found. Comparison of the protein solubility shifts in lysate vs. living cells highlighted the targets directly interacting with the compounds. As PISA analysis is now joining the arsenal of fast and reliable target characterization techniques, the presented database, ThermoTargetMiner, will become a useful resource in lung cancer research.

Introduction

Lung cancer is one of the most prevalent cancer types. It remains the essential contributor to cancer-related deaths globally, with approximately 2.2 million new cases every year resulting in 1.8 million deaths worldwide[1]. There are two main forms of primary lung cancer, classified by the type of cells that initiate it. Non-small-cell lung cancer (NSCLC) is the most common form corresponding to 85% of all cases. NSCLC is, in turn, divided into 3 types: squamous cell carcinoma, adenocarcinoma and large cell (undifferentiated) carcinoma[2]. Adenocarcinoma and large cell carcinoma form peripheral nodules and masses, while squamous cell carcinoma is central and endobronchial. Small-cell lung cancer (SCLC) accounts for the rest of lung cancer cases and exhibits neuroendocrine properties. Being strongly associated with tobacco exposure, it is highly aggressive and rapidly growing. About two-thirds of lung cancer patients have metastasis at the time of diagnosis[3].

Small-molecule chemotherapy is the main approach to managing lung cancer, although the initial treatment is stage-specific. Surgery can effectively manage tumor removal for the majority of early-stage NSCLC[4]. Chemotherapy delivered before or after surgery (also known as neoadjuvant and adjuvant chemotherapy) is widely used in stage II and stage III NSCLC. Chemotherapy typically serves as the primary approach for metastatic NSCLC. Recently, definite chemoradiotherapy combined with immune checkpoint inhibitors (ICIs) administration has become the preferred treatment for unresectable stage III NSCLC. For SCLC, localized cases are usually treated with surgery and concurrent chemoradiotherapy[3]. Adding ICIs to the conventional first-line platinum-based chemotherapy is the recommended approach for treating newly diagnosed metastatic SCLC.

The survival in lung cancer, especially for advanced-stage cases, is relatively poor. The 5-year survival of NSCLC is around 60-70% for stage I of development, 40-50% for stage II, 5-25% for stage III and less than 1% for stage IV[2] . SCLC is characterized by its poor prognosis and remarkable tendency for early metastasis. Most patients respond to treatments only temporarily, which leads to a median survival of less than two years for those with early-stage SCLC and around one year for those with metastatic disease[3].

Due to the limited survival of lung cancer patients, there is an urgent need for new drug development in this area. In April 2024, there were 317 registered small molecule drugs for lung

cancer and 2795 registered clinical trials for such drugs on http://clinicaltyrials.gov. Over 70% of the clinical trials were in phase II and phase III.

The primary reason for failure in both phase II and phase III is drug inefficiency [5]. In many cases this failure is due to the poor knowledge of the drug action mechanism. The latter implies possessing solid information on drug targets, including the residence time of the drug on its target[6]. Another important reason for clinical trial failure is unacceptably high drug toxicity, resulting from the engagement of unintended targets (off-targets) by the drug or its metabolites [7,8]. Therefore, the pharmaceutical industry pays great attention to thorough in-vitro target characterization before in-vivo clinical trials. Several complementary analytical techniques are employed for this purpose, at a rather high cost. To reduce the expenses and speed up drug development, the techniques for drug target characterization should combine the reliability of produced results with a reasonably high throughput. Another important desirable aspect of analysis is its proteome-wide nature, to reduce the risk of overlooking important (off-)targets.

In the last 10-15 years, several system-wide methods for dissecting drug targets have emerged. A well-known approach to probing drug-target interactions, thermal stability shift assay[9,10], has been expanded to complex in-vitro and even in-vivo settings, while its first implementation, cellular thermal shift assay (CETSA[10]), required *a priori* knowledge of the target. The latter drawback was overcome in Thermal Proteome Profiling (TPP[11] or MS-CETSA[10]) that employs mass spectrometry (MS) for a system-wide search of target candidates. These techniques detect the change in the melting temperature of a target protein upon binding to a small molecule. The main bottleneck of these MS-based approaches was their low throughput. In contrast, Proteome Integral Solubility Alteration (PISA) assay[12], which analyzes the shift in protein solubility rather than that in melting temperature, offers at least an order of magnitude higher throughput. On top of that, PISA provides the possibility to employ different solubility modulators besides elevated temperature[12], such as, e.g., organic solvents[13] and kosmotropic salts[14]. When applied to a cell lysate, all the above approaches will highlight the proteins that bind directly to the drug, while the application to living cells also reveals the downstream proteins as well as the targets of drug metabolites[15].

We have previously applied PISA for protein target identification and exploring mechanisms of small-molecule drugs[6,12], biomarker discovery[16], as well as for identification and

prioritization of enzyme substrates[15,17]. In the current study, we tested the PISA performance as a higher-throughput technique for reliable drug target deconvolution on a larger set of drugs, choosing lung cancer as the application field (**Figure 1**). For that purpose, we selected 67 therapeutic agents specifically designed or repurposed for lung cancer treatment and included as disease models both NSCLC and SCLC cell lines (A549 and NCI-H82 cells, respectively). Both the cell lysates and intact cells were treated by each drug and vehicle as control, PISA-processed, after which the proteomes were extracted and analyzed by a combination of liquid chromatography and tandem mass spectrometry (LC-MS/MS). The shifts of the protein PISA signals quantified using the tandem mass tag (TMT) were then analyzed. From the previous similar efforts with drug target identification by expression proteomics[18], we expected that the datasets for the drugs with the same target would be found to be co-localized in hierarchical clustering, revealing similar drug mechanisms. However, in the PISA data drugs with the same target did not necessarily cluster together, which complicated the action mechanism determination. We then employed orthogonal partial least squares-discriminant analysis (OPLS-DA), contrasting each drug treatment with all other conditions, as was previously performed in expression proteomics[18]. But OPLS-DA of PISA results revealed very few significantly shifting proteins, again in stark contrast with expression proteomics[19]. These puzzling results called for innovative approaches to PISA data processing for reliable identification of the drug targets.

We addressed this unexpected problem as follows. First, from the distribution of proteins' main OPLS coordinates we estimated for each protein the p-value of being a statistical outlier in that distribution. Then, using the fact that each TMT set had a sample treated with a control drug methotrexate (MTX), a p-value threshold was chosen so that all such samples co-localized most tightly in hierarchical clustering. The outliers in the samples treated with other drugs (typically ≈5% of all quantified proteins) were then considered candidate targets ('pro-targets') of a given drug. For validation of the target candidates, we examined the whole dataset: if the same candidate appeared for the same drug in a different type of PISA sample (lysate vs. in-cell, or NSCLC vs SCLC cells), it was considered validated.

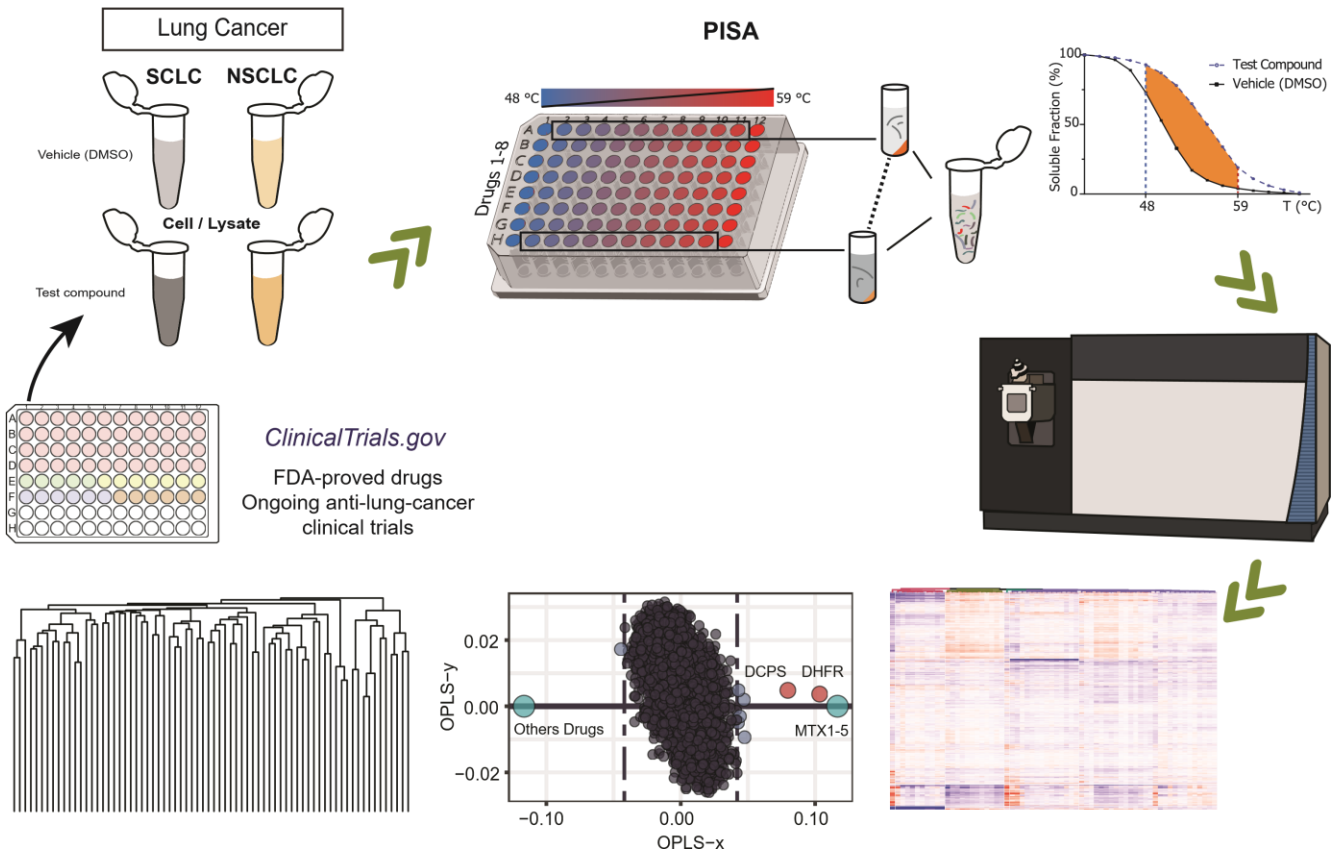

Figure 1. Workflow for PISA-based target identification. The drugs with various known targets and potential mechanisms were chosen from the ongoing chemotherapy-based lung cancer clinical trials. SCLC and NSCLC cell lines were selected as the disease model. PISA analysis was performed both in cell lysate and intact cells. After thermal treatment and ultracentrifugation, proteins were digested, and peptides were labeled with TMT. Samples were then pooled and analyzed by LC-MS/MS. The protein PISA signal shifts compared to vehicle-treated control were visualized on a heat map and processed by OPLS-DA. Upon choosing a proper threshold, a statistical model based on the main OPLS-DA coordinate was used for identification of potential protein targets and hierarchical clustering of the drugs.

Results and Discussion

PISA analysis

After the selection of cell lines and drug panel (see methods), cells and cell lysates were treated with the drugs and PISA-analyzed. The number of proteins identified in at least one PISA analysis in A549 cell or lysate samples was 10,632, out of which 9,570 proteins were quantified with at least 2 peptides, excluding potential contaminants. For the H82 cell line, 10,823 proteins and 9,736 proteins were quantified, respectively.

Figure 2 shows the Venn diagram of the overlap between all four datasets encompassing 15 TMT sets. On average, 44% of the proteins detected without missing values were common in all datasets. In A549 cell lysate and cells, 5,063 and 4,626 common proteins were quantified, respectively, while the respective numbers for H82 were 5,650 and 5,756 proteins.

In the first round of analysis, three biological replicates were used to determine the fold-change of the PISA shifts and the respective p-value for each protein under each drug/vehicle condition. By combining log2 transformed fold-changes and -log10 transformed p-values, we generated four volcano plots for each drug (**Supplementary Figure 1-71**). The common proteins in a dataset were used for creating a heatmap by hierarchical clustering. As an example, **Figure 3A** shows a heatmap for the shared proteins from A549 lysate. Heatmaps for the other datasets are shown in **Supplementary Figure 72-73.** The first look at the heatmap revealed the already mentioned problem – not all drugs with common known targets co-localized on that heatmap. For instance, selumetinib, trametinib, and binimetinib that all target MEK (MAP2K) were not found in close proximity to each other. At the same time, the PISA shifts of MAP2K1 and MAP2K2 for the three drugs were both strong and statistically significant (**Table 1**), which testifies to the validity of the PISA analysis.

Table 1. Fold-changes in PISA and the corresponding p-values of MEK proteins in A549 lysate treated with selumetinib, trametinib or binimetinib vs. DMSO.

	Selumetinib		**Trametinib**		**Binimetinib**	
	Fold-change	p-value	Fold-change	p-value	Fold-change	p-value
MEK1 (MAP2K1)	2.3 ± 0.2	2.4×10^{-3}	2.1 ± 0.1	3.5×10^{-4}	2.4 ± 0.1	1.6×10^{-4}
MEK2 (MAP2K2)	3.8 ± 0.4	4.9×10^{-3}	2.4 ± 0.3	1.8×10^{-2}	4.3 ± 0.5	5.7×10^{-3}

Examination of the MTX-treated samples (the positive control in each experiment) revealed that they did not cluster together either. The cause of the problem was the specificity of the solubility shift in PISA that affected very few target proteins, while the shifts in the absolute majority of proteins were to a large extent due to statistical fluctuations. Removing this noise and "purifying" the true targets turned out to be a nontrivial but necessary task.

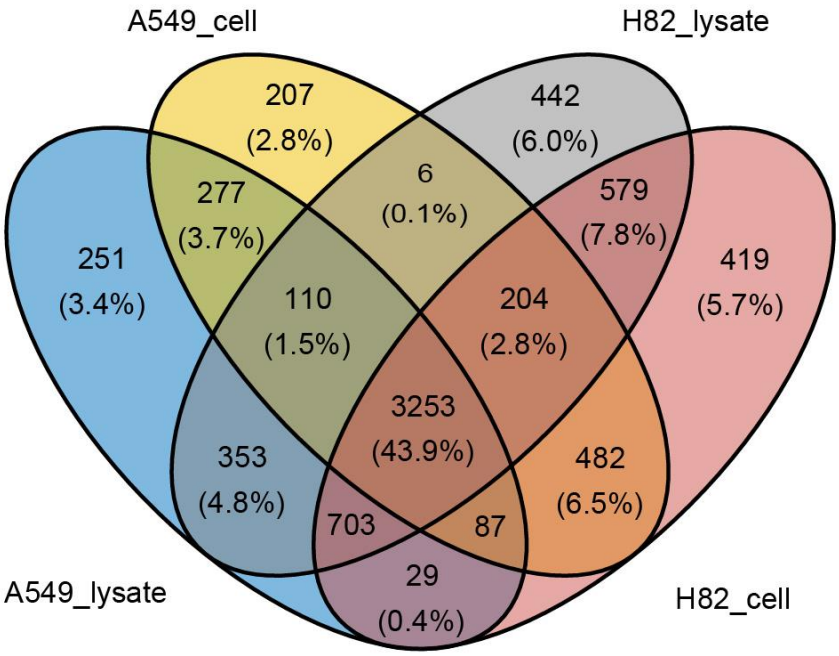

Figure 2. Number of proteins identified in all four PISA datasets and their overlap. 3253 proteins (expected number is 1872) without missing values were shared across four datasets.

Optimal p-value threshold

To address this problem, we first applied the OPLS-DA analysis that has demonstrated its utility in the ProTargetMiner expression proteomics database of drug target candidates[18]. Here, the PISA shifts for each drug of interest were contrasted with those for all other drugs and controls (an example for olaparib is shown in **Figure 3B**, lower panel). The coordinates of each protein along the main axis correspond to a specific solubility increase with drug treatment (positive values) or its decrease (negative values). Compared to the raw PISA shifts, the main OPLS-DA coordinates provide an enhanced specificity, as the shifts common for many drugs obtain a relatively small coordinate value compared to the shifts of similar magnitude that are specific for a given treatment [18]. We thus expected that the main OPLS-DA coordinate would provide more meaningful clustering of the treatments. There was indeed an improvement, but not sufficient, as the sporadic PISA shifts of unrelated proteins were still posing a problem. It became clear that these unrelated proteins needed to be down-prioritized, so that only proteins passing a certain threshold for statistical significance (outliers) would be used for clustering.

In order to identify the threshold for such statistical outliers, a distribution of the OPLS-DA coordinates was assessed for each model. One example is the OPLS-DA model comparing olaparib vs. all other drugs treated H82 intact cells (**Figure 3B**). The dispersion of OPLS-DA coordinates was determined, and the p-value for each outlier was calculated using the error function. The latter assumed Gaussian distribution, but the exact shape of the distribution was not critical for the final results. The horizontal axis was then transformed into -log10(p) values (**Figure 3C**).

Our strategy was to use in further data processing only the PISA shifts for the outliers, zeroing all other PISA shifts that were assumed to be noise. Such an approach required evidence-based determination of the optimal threshold for p-values (dashed vertical line in **Figure 3C**). For the threshold determination, we used the data on MTX-treated samples that were present in all individual TMT sets (5 such samples in each PISA analysis type). A figure of merit (FoM) function was created corresponding to the average distance in all four types of PISA analysis between the positions of the neighboring MTX samples in hierarchical clustering of all samples of a given type. The tighter the cluster that MTX-treated samples created, the lower FoM was obtained. As **Figure 3D** shows, the minimal FoM is observed at the value of 4.5. This value was accepted as the optimal

-log10(p) threshold for the whole dataset, and the outlying proteins exceeding this threshold, as in **Figure 3C**, were taken as pro-targets (drug target candidates).

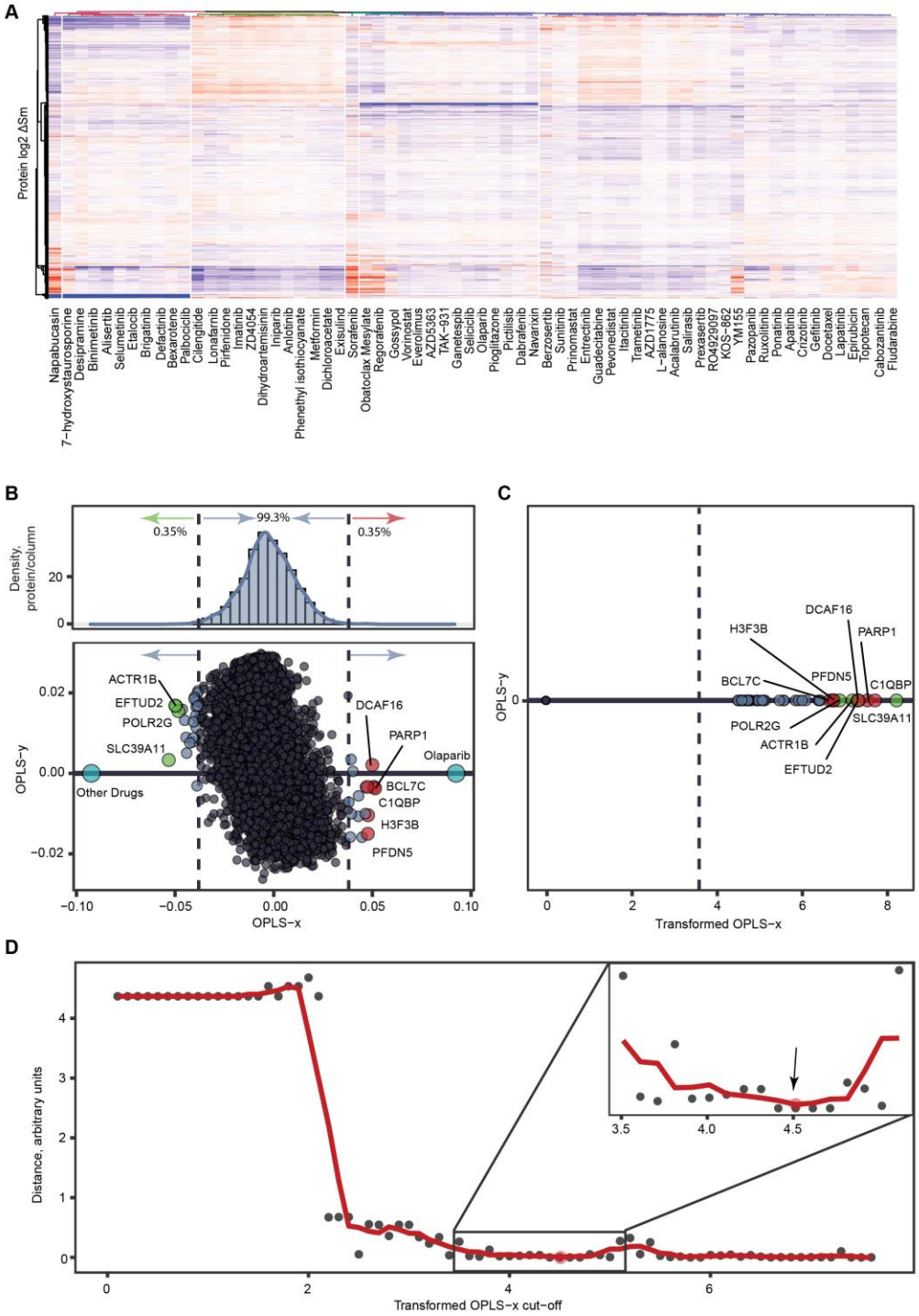

Figure 3. Data processing for drug target identification. A. Heatmap based on clustering of log2 transformed PISA fold-changes for 4,626 shared proteins in the A549 lysate dataset. **B.** Lower

panel: The loading plot of an OPLS-DA model comparing olaparib to all other drugs in H82 cell dataset. Upper panel: the density distribution of protein's x-coordinates in the loading plot. Olaparib's known target PARP1 exhibits the next-highest x-coordinate. **C.** The transformed x-coordinates correspond to -log10(p) of the 39 proteins above the threshold value (dashed vertical line). The top 10 proteins are represented as red/green circles if they became more/less soluble upon olaparib treatment. **D.** Selection of the optimal cut-off threshold. Distance is the average distance between control MTX datasets in hierarchical clustering of all data. Insert shows that the curve reaches its minimum at x=4.5, chosen as optimal cut-off value.

Drug clustering

With the PISA shifts of all below-threshold proteins set to zero, the hierarchical clustering data became much more meaningful. While the MTX samples clustered tightly as expected (see **Figures 4A, B** as examples), many drugs with similar targets were also found close together. For example, in the A549 lysate dendrogram, the three MEK inhibitors, selumetinib, trametinib and binimetinib, are found next to each other, similar to the potent PTK2 inhibitors brigatinib[20] and defactinib[21]. With a meaningful clustering achieved, we moved to the identification of the pro-targets and their validation.

Drug target candidates (pro-targets)

With the optimal threshold of 4.5 for -log10(p), the median number of target candidates for different drugs was 27.5 for A549 lysate and 20 for intact A549 cells, while for H82 cells the median numbers were 24 and 43, respectively. These numbers represent 6.0% of all quantified proteins for A549 lysate and 4.0 % for intact A549 cells, as well as 4.2% for H82 cell lysates and 7.5% for intact cells. For pro-target validation, we applied the following principle: if the same candidate appears in k>1 dataset for the same drug, it is considered validated at the k-th level. All validated pro-targets of 67 drugs are listed in **Table 2**. On average, we found 3 pro-targets per drug with k=2 (overlaps in two datasets), 0.4 pro-targets with k=3 and 0.2 pro-targets with k=4. For control of the false discovery rate (FDR), the 'candidates' were selected at random; the numbers of such spurious overlaps were 1.3 proteins with k=2, 4.4×10^{-3} with k=3 and 5.5×10^{-6} with k=4.

While these numbers indicate that, strictly speaking, only pro-targets with k≥3 are statistically reliable, we decided to consider also the pro-targets with k=2 to minimize the number of false negatives. The pro-targets shared between the lysate and intact cell analysis of the same cell line, which is a more reliable subset of k=2 pro-targets, are shown in **Supplementary Figure 74-145**.

As an example of pro-target analysis, pevonedistat (also known as MLN4924) treatment in A549 lysate produced 127 target candidates, 18 candidates for intact A549 cells, 45 for H82 lysate and 66 for intact H82 cells (**Figure 4C**). Of these, 11 pro-targets were found in 2 datasets. Importantly, 2 candidates (NAE1 and UBA3) were found in all 4 datasets, while the anticipated number of randomly shared proteins for k=4 is only 1.7×10^{-5}. These two proteins, NAE1 and UBA3 (the latter is also known as NAE2), are two subunits of the known target of that drug - NEDD8-activating enzyme E1 (NAE)[22]. Seven other proteins were shared in two PISA analyses of intact cells. Of these, DCAF7, CRBN and CTNNB1 are found to be co-expressed with NAE[23].

Another notable example is ganetespib (STA9090), for which 33, 41, 21 and 33 targets candidates were found in the four datasets, respectively. Of these, 9 proteins (expected number – 0.8) were shared in 2 datasets, 1 protein (2.3×10^{-3} proteins expected) in 3 datasets and 2 proteins, HSP90 subunits HSP90AA1 and HSP90AB1, were shared in all datasets (expected number - 2.3×10^{-6}). As ganetespib is designed to be an HSP90 inhibitor[24,25], this result clearly demonstrates the analytical power of the ThermoTargetMiner approach in drug target identification.

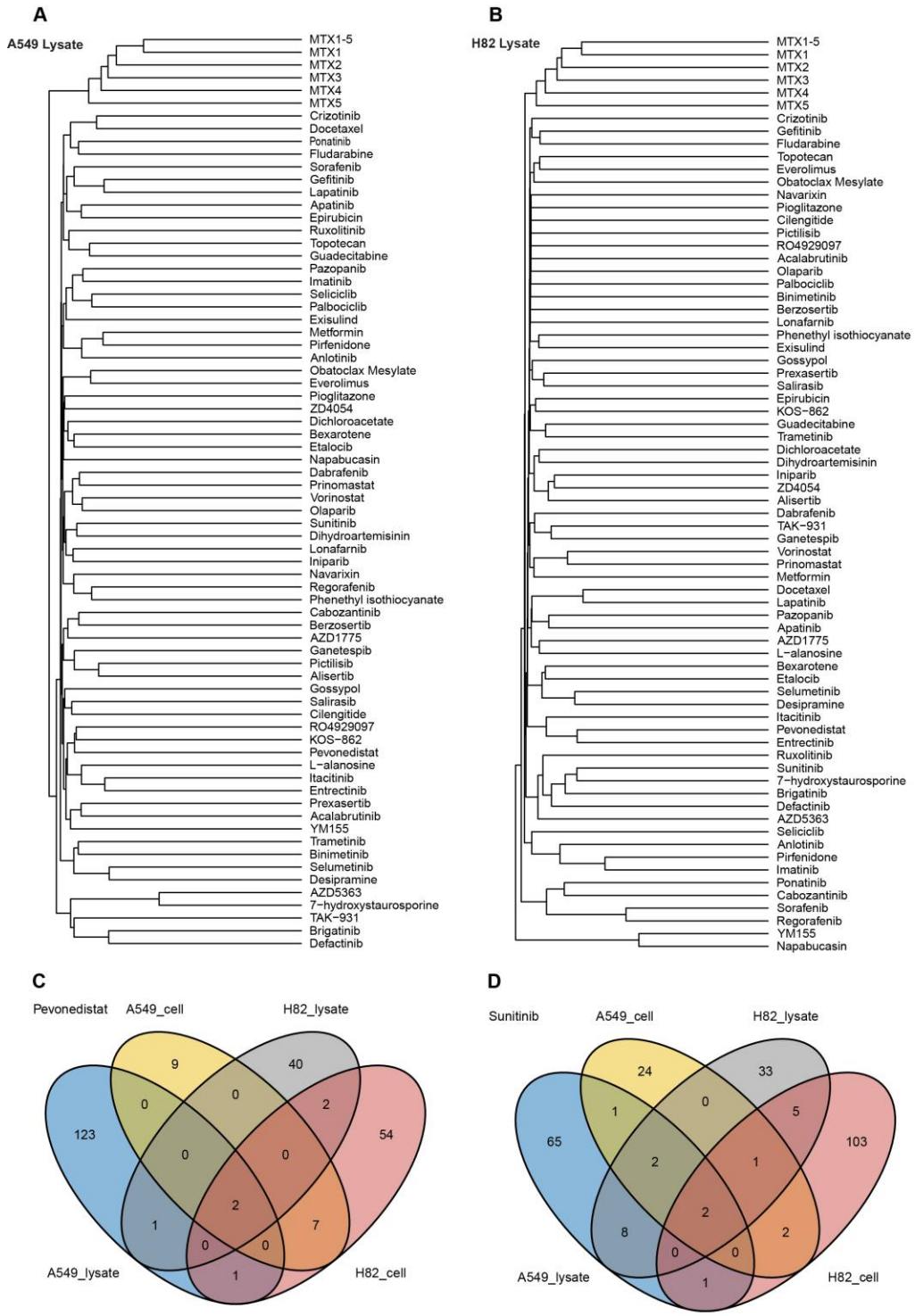

Figure 4. Pro-target-based clustering of the PISA datasets from drug-treated samples together with all MTX-treated controls from the lysates of A549 (**A)** and H82 (**B**) cells upon application of the common optimal threshold of 4.5. Venn diagrams show the overlap of the identified pro-targets of pevonedistat (**C**) and sunitinib (**D**).

These and other target candidates are listed in **Table 2**. The largest number of PISA datasets (20 in total) was obtained for MTX. The DrugBank[25] lists three MTX targets: TYMS, ATIC, DHFR. Of these, only DHFR is consistently revealed as a pro-target by ThermoTargetMiner. TYMS is an outlier in the MTX-treated intact cells, but not in lysates (**Figure 5**), which is similar to our previous PISA results[12]. ATIC showed a similar tendency. An explanation for the phenomenon is that, unlike direct binding of MTX to DHFR, MTX needs first to be transformed into MTX polyglutamates (MTXPGs) to exert effects on TYMS and ATIC[26]. Apparently, MTX binding to TYMS and ATIC requires intact cellular environment which provides functional enzymes and substrates. This result confirmed the sufficiently high reliability of the pro-targets identified by PISA for the ThermoTargetMiner database.

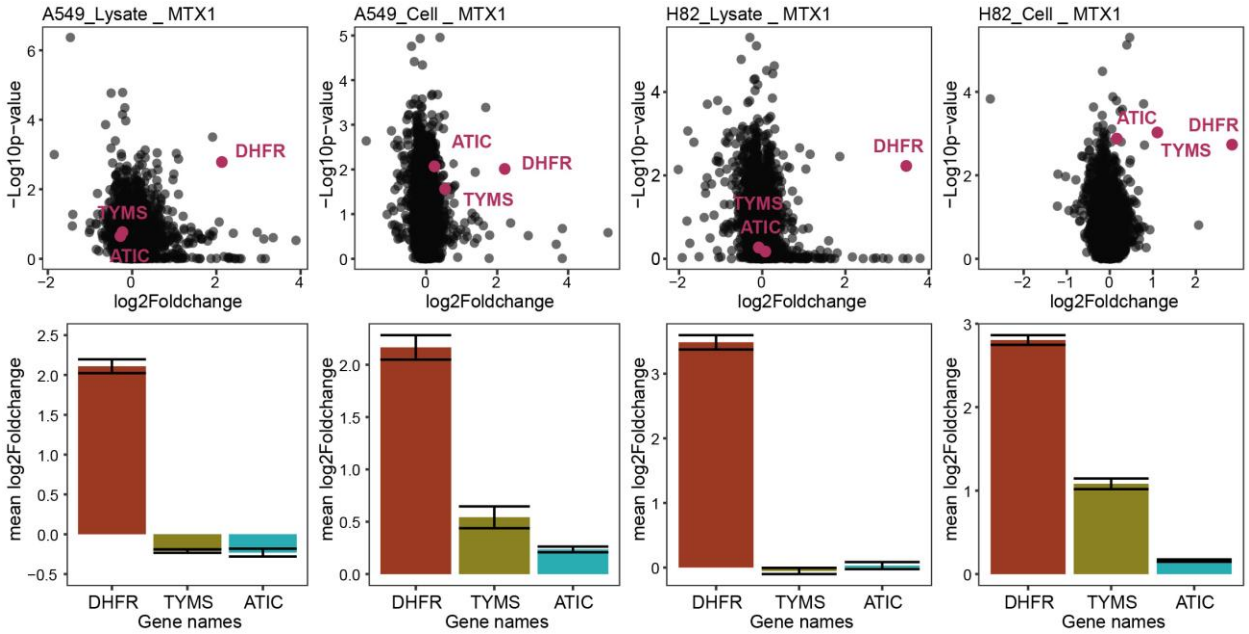

Figure 5. Fold-changes in PISA and p-values of the three MTX targets listed in Drugbank [25]: DHFR, TYMS and ATIC.

Novel targets

Sunitinib is designed to target receptor tyrosine kinases (RTK), such as vascular endothelial growth factor (VEGF) receptor and platelet-derived growth factor (PDGF)[27]. However, these

transmembrane proteins were not identified in our PISA analysis, likely due to their poor solubility. Instead, 22 other proteins were shared between at least two datasets (**Figure 4D**). Among these pro-targets, NMT1 and NMT2, which have been found overexpressed in cancers and thus hinted to be potential anticancer targets[28], were found in 4 and 3 ThermoTargetMiner datasets, respectively. Previous work[18] of our group has discovered that sunitinib treatment induces significant NMT1 downregulation, supporting the current PISA finding.

Another protein that exhibited significant PISA shift in all four sunitinib datasets was TTC38 (tetratricopeptide repeat domain 38), which has not been linked to sunitinib binding. Given the very low *a priory* probability of being an outlier with k=4 (only 3.7×10^{-5} such events are expected by pure chance), it is highly likely that TTC38 is a cognate target of sunitinib. To a large extent, the same applies to CAMK2D which was significantly solubilized by sunitinib treatment in three out of four datasets. Of relevance is that the activity of the related protein CaMKII has been significantly elevated following chronic sunitinib treatment, which suggested a mechanism for sunitinib-mediated cardiovascular dysfunction[29]. Furthermore, our results validated the previously reported sunitinib binding to STK24[30], AAK1[31], CSNK1A1[32], RPS6KB1, STK3, and STK4[33].

Phenethyl isothiocyanate (PEITC) is a natural anti-cancer compound that is present in many cruciferous vegetables. It is believed to suppress cancer progression through diverse mechanisms like cell cycle arrest at the mitotic phase and induction of apoptosis[34]. On the molecular level, PEITC hinders tubulin polymerization and alters tubulin secondary and tertiary structures[35]. However, there is no validated target of PEITC in the Drugbank[25]. In ThermoTargetMiner, PAFAH1B3, one of the most frequently overexpressed metabolic enzymes in human tumors[36], is found as the sole pro-target across all four datasets (the expected number of such events is 6.7×10^{-6}). Also, tubulin-specific chaperone D (TBCD) that plays a crucial role in tubulin complex assembly[37], was an outlier in three datasets (6.3×10^{-3} such events are expected). TBCD is a validated pro-target of one other drug in our database. The drug is KOS-862 (also known as epothilone D or desoxyepothilone B), a tubulin stabilizer known to arrest the cell cycle at the mitotic phase[38]. Interestingly, the effect of KOS-862 on microtubules is opposite to that of PEITC: while PEITC blocks microtubule polymerization[35], KOS-862 promotes the latter process, facilitating the formation of multipolar spindles[38]. Consistent with that, in PISA analysis these two

drugs demonstrate opposite effects on TBCD's solubility: PEITC treatment increases it, whereas KOS-862 lowers TBCD's solubility.

Mechanism of action

Napabucasin (BBI-608) is a novel STAT3 signaling inhibitor that binds to STAT's hinge pocket and diminishes STAT3 DNA binding affinity[39]. In ThermoTargetMiner, multiple oxidative stress-related proteins, including ADO, ADI1, PRDX5 and ETHE1, showed significant solubility alteration in at least three datasets. Moreover, napabucasin impacted two pivotal regulators of redox homeostasis in humans, thioredoxin and the glutathione system[40], as both thioredoxin reductase TXNRD2 and glutathione peroxidase GPX1 demonstrated decreased solubility in the two cell lysates. Therefore, we hypothesized that napabucasin acts as an anticancer compound by inducing oxidative stress on cancer cells.

To test this hypothesis, we performed GO enrichment analysis on the PISA data from napabucasin treated A549 cells. The response to oxidation was found to be the most significantly involved biological process (**Figure 6A**). In agreement with that, it has been reported that napabucasin's induction of ROS in multiple cell lines[41] is one of the anti-tumor action mechanisms of this drug. In the same study, napabucasin was found to be a substrate of another oxidoreductase, NAD(P)H dehydrogenase [quinone] 1 (NQO1)[41]. In our A549 lysate and intact cell data, NQO1 was one of the most shifting proteins (**Figure 6B and 6C**). In H82 data, NQO1 was not quantified, possibly because its transcription level in A549 cells is much higher than that in H82 cells (2554 vs. 12 transcripts per million)[42,43]. In addition to NQO1, multiple key proteins responsible for the maintenance of cellular redox homeostasis, such as PRDX5, PRDX6 and GPX2 were among the top 0.6% shifting proteins in napabucasin-treated A549 intact cells, and in A549 lysate, the p-values of GPX1 and NQO1 ranked as 10th and 11th lowest, respectively.

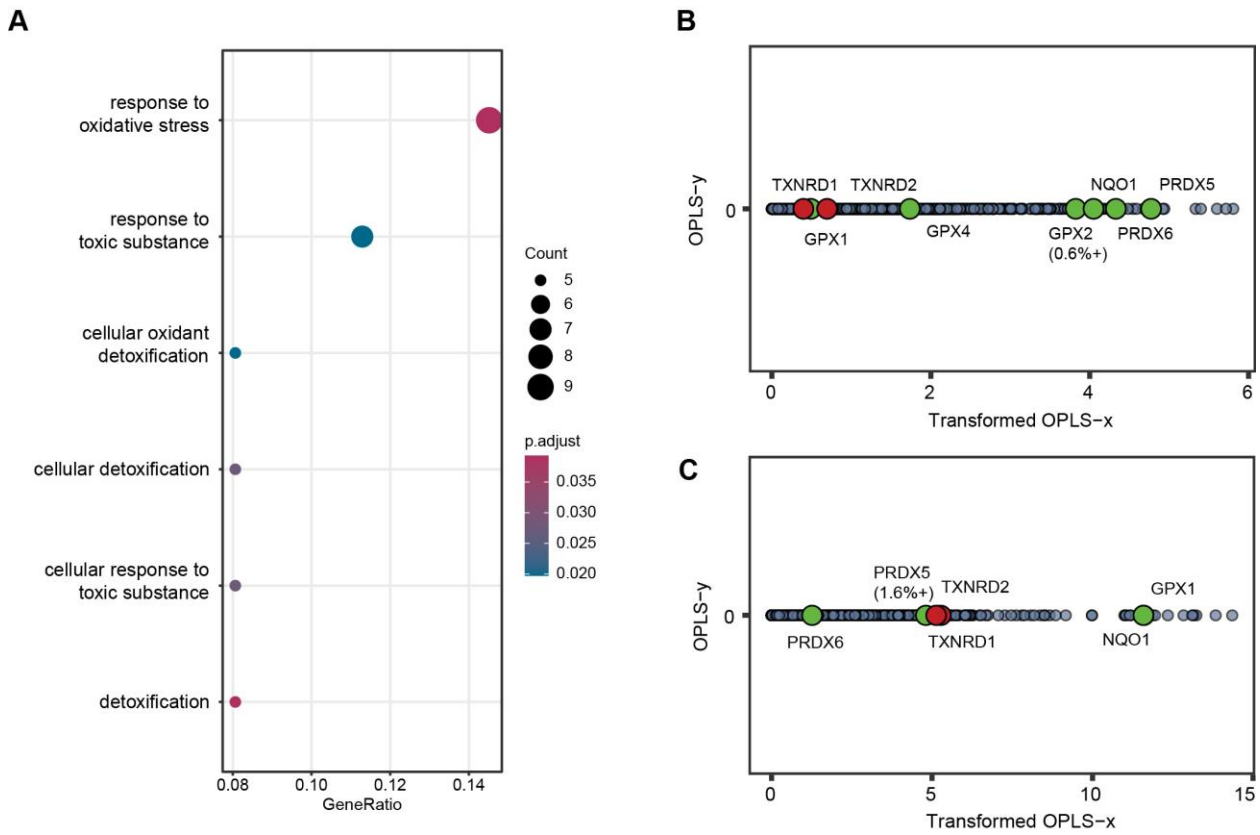

Figure 6. A. GO term enrichment in biological pathways of 66 proteins that pass the threshold value of 3 (top 1.4%) in napabucasin treated A549 cells. **B.** Positions on the transformed opls-x scale for A549 cells of the proteins involved in cellular redox homeostasis**. C**. Same for A549 lysate.

Table 2. The list of pro-targets validated through our data and ProTargetMiner[18] for 67 compounds profiled in this study along with clinical phase information and targets of these compounds in DrugBank [25].

Drug name	Clinical Trail Phase	Known Targets in DrugBank	Position in %% from top (+) or bottom (-) in ProTargetMiner [18]	Pro-targets (shared in 4 TTM datasets, 3 datasets, and 2 datasets in **cell** or only in lysate)
7-hydroxystaurosporine	2	PDPK1		ROCK1[44], STK3[44], **STK4** [44], **MAP2K6, GSK3B**, PRKCI, CTPS1, **PRKAR2A**, PAK4 [44], **CAMK2D** [44]
Acalabrutinib	2	BTK		**CIRBP**
Alisertib	2	AURKA		SPR, ATIC[45], IDH1[45], IVD
Anlotinib	3	KIT, VEGFR, PDGFR, FGFR		**BICD2**, AFTPH, **CHAF1B**, **PDE6D**, **ASAH1**
Apatinib	4	KDR		**ANAPC5**
AZD1775	2	WEE1		CLPP, ECH1, **ADK**
AZD5363	2	AKT		**QTRT1**, MAP2K6
Berzosertib	2	ATR, ATM		**PIP4K2C, PIP4K2B, CTSC, GSK3A, PSIP1**
Bexarotene	3	RXRA, RXRB, RXRG		XPO7, ACAD9, TFB2M, CSE1L, GSTM2, SARS2
Binimetinib	2	IL6, TNF, IL1B, MAP3K1, MAP2K2		
Brigatinib	3	ALK, EGFR, ABL1, IGF1R, FLT3, INSR, MET, ERBB4, ERBB2		**DUSP23, PTK2**[20], DNAJC13
Cabozantinib	2	MET, KDR, RET	GLUD1 (1.0%+)	PIP4K2C[46], GLUD1
Cilengitide	2	?		WDR5
Crizotinib	3	ALK, MET		**HEBP1, ASAH1**
Dabrafenib	4	BRAF, RAF1, SIK1, NEK11, LIMK1		PMPCA, CDK5[44], CSK[44], **ENO1**, RNMT, **CDK2**[44]
Defactinib	2	PTK2		**PTK2**[21], CDK5, RPS6KA3, MAPK1[47], MAPK3[47], PDXK
Desipramine	2	SLC6A2, ADRB2, SLC6A4, HTR2A, ADRB1, SMPD1, HRH1, CHRM1, CHRM2, CHRM3, CHRM4, CHRM5, HTR1A, HTR2C, DRD2		
Dichloroacetate	2	?		
Dihydroartemisinin	2	?		**WDR54, PTGR2, HS1BP3**
Docetaxel	2	TUBB1, BCL2, MAP2, MAP4, MAPT, NR1I2,		
Entrectinib	2	NTRK1, NTRK2, NTRK3, ROS1, JAK2, TNK2		DPH5, **PLIN2, PTAR1, PTK2**[48], **IGF1R** [48]
Epirubicin	3	TOP2A, DNA	SSRP1 (3.6%-)	SSRP1, **FAU**
Etalocib	2	LTB4R, PPARG		NIPSNAP1, HIBCH, **HADHA**
Everolimus	3	MTOR		UBQLN1, UBQLN4, **GLMN**, MTOR[49], ZWINT

Exisulind	2	PDE4D, PDE4C, PDE5A, PDE2A, GSTP1, AKR1B1, AKR1B10,		DPP3, **ZYG11B**
Fludarabine	2	RRM1, POLA1, DNA, DCK,		**NUDT4**
Ganetespib	2	HSP90		PA2G4, **CHORDC1,** TP53RK, **HSP90AB2P**[24], **HSP90AB4P**[24], YARS, SPR, HSP90B1[24], **HSP90AB1**[24]**, HSP90AA1**[24]**, CEP112**
Gefitinib	3	EGFR		**FAM96B**[50]**, CORO1C**
Gossypol	3	BCL2L1		HYOU1, PPCS, IWS1, CHAMP1, GMPPA, SETD7, **PITRM1**, KARS, RCN2, EIF3A, G3BP1, HMGCS1, **PCYT1A**, ACADSB, PSMC4, MSH2, LRPPRC, GTF2E2, NSF, EWSR1
Guadecitabine	2	DNMT		QTRTD1, PGM1, **CSTA**
Imatinib	2	BCR, KIT, RET, NTRK1, CSF1R, PDGFRA, DDR1, ABL1, PDGFRB		
Iniparib	2	?		
Itacitinib	2	JAK1		DPH5
KOS-862	2	TUB		**DLGAP4,** SLIRP, **TBCD,** RABGGTA, PITRM1, **LGALSL, CAMSAP2, PDE6D**
L-alanosine	2	ADSS, ADSSL1, pyrB		
Lapatinib	2	EGFR, ERBB2		ZYG11B, **FECH**
Lonafarnib	3	FNTA, FNTB		TIAL1, **FNTA**[51]
Metformin	2	PRKAB1, ETFDH, GPD1, MTOR		**COPS7A**
MTX1-5	4	TYMS, ATIC, DHFR		DCPS, **GSS, DHFR**[52]**, DCK**[53]
Napabucasin	3	?		XPNPEP1, C12orf10, CAAP1, NLN, **ADI1**, MRI1, **ADO**, COA7, NHLRC2, MVK, **PRDX5**[54]**, MPST**, DTYMK, IMPDH2, HARS, APP, **ETHE1**, HAT1, CTSD, TXNRD2, GPX1[55]
Navarixin	2	CXCR1, CXCR2		
Obatoclax Mesylate	3	BCL2		**NUP133, NUP107, HADHB, NUP98**, CARS
Olaparib	3	PARP1, PARP2, PARP3		**PARP1**[56]
Palbociclib	2	CDK4, CDK6		**NUDT1**, CDK4[57]
Pazopanib	2	FLT1, KDR, FLT4, PDGFRA, PDGFRB, KIT, FGFR3, ITK, FGF1, SH2B3		ETNK1, CMBL, ECH1, CHKA, **STX2**
Pevonedistat	2	NAE		**ANAPC4, KLHL11, ETNK1, UBA3**[58]**, KCTD9, KCTD1, MORF4L2, NAE1**[58]**, DCAF7, CTNNB1, POLD1, CRBN**
Phenethyl isothiocyanate	2	?		**POLDIP2, USP22**, FN3K, **TBCD**[59]**, IPO4, HEATR3, PAFAH1B3**, ALDH9A1, **HTT, ALDH1B1**[60], ME2, PHGDH, **CLUH**

Pictilisib	2	PIK3AP1		**PIK3R1**[61]
Pioglitazone	2	PPARG, MAOB		ADH5
Pirfenidone	4	FURIN		
Ponatinib	2	ABL1, BCR, KIT, RET, TEK, FLT3, FGFR, FGFR2, FGFR3, FGFR4, LCK, SRC, LYN, KDR, PDGFRA	SLK (0.1%-)	**SLK**[62]**, CDK5, CSK**[63]**, DCK**, MAP4K4
Prexasertib	2	CHEK1		**FECH, PAK4**
Prinomastat	2	MMP		XPNPEP1, ZDHHC5, PMPCA, RAB4A, **IMPA2**
Regorafenib	3	FLT1, KDR, FLT4, KIT, PDGFRA, PDGFRB, FGFR1, FGFR2, TEK, DDR2, NTRK1, EPHA2, RAF1, BRAF, MAPK11, FRK, ABL1, RET		CDK12, GSK3B, ALDH1B1, ALDH2, PDE6D
RO4929097	2	PSENEN, APH1A, APH1B		**DPP8, RPS21, SH3BGRL**
Ruxolitinib	2	JAK2		
Salirasib	2	ICMT		
Seliciclib	2	CDK1, CDK2, CDK7, CDK9, MAPK1, MAPK3, CSNK1E		
Selumetinib	2	MEK1, MEK2		
Sorafenib	2	BRAF, RAF1, FLT4, KDR, FLT3, PDGFRB, KIT, FGFR1, RET, FLT1		RNMT
Sunitinib	2	PDGFRB, FLT1, KIT, KDR, FLT4, FLT3, CSF1R, PDGFRA	NMT1(0.1%-)	**BCLAF1, AHCTF1, TTC38**, STK3[33], STK4[33], RPS6KA3, CSNK1A1[32], **NMT1**, RPS6KB1[33], **NMT2**, NME4, **CAMK2D, STK24**[30]**, AAK1**[31]
TAK-931	2	CDC7		RIOK1, TP53RK, PRPF4B, CSNK1A1, CSNK2A2
Topotecan	3	TOP1, TOP1MT, DNA	CBR3 (4.4%-)	CBR1, CBR3
Trametinib	4	MAP2K1, MAP2K2		THEM4, **MAP2K1**[64], PRMT5
Vorinostat	2	HDAC1, HDAC2, HDAC3, HDAC6, HDAC8, acuC1		HDAC6, XPNPEP1, **GPATCH1**, HDAC2[65], HDAC1, MTA2
YM155	2	BIRC5		UQCRFS1, CSTB
ZD4054	2	EDNRA		

Discussion

Identifying drug targets is crucial in drug discovery and development. Direct / affinity-based methods are widely used to validate the physical binding of a drug to its target. These methods usually require modification of the drug or the target protein. In addition, direct affinity-based methods lack an intracellular environment. Without the existence of protein complexes, the proteins' structures can be different, thus, the direct bindings between small molecules and proteins are less trustworthy. Moreover, off-target effects are not considered in such experiments, resulting

in a lack of knowledge of the drug's potential side effects. Compared to other target identification technologies, proteomics methods do not require the target proteins to be abundant, synthesized probes or pull-downs. Especially, PISA can demonstrate drug-protein interactions in a protein-complexes-containing environment. This unbiased assay increased the efficiency by an order of magnitude compared to TPP, providing a relatively economic solution for finding drug on-target and off-target engagements.

ThermoTargetMiner provides a universal analytical methodology for large-scale PISA data. For a long time, PISA has been used for studies that only include a few conditions and the data was processed by computing fold-changes and p-values. The rationale for applying the same data processing approach to more complex data remains to be verified. Two research groups have tried to push PISA to large-scale experiments. Olsen group used q-value ≤ 0.05 and an absolute log2-transformed fold-change ≥ 0.5 as the cut-offs[66]. Alternatively, Gygi group acquired data from two replicates and chose cut-offs based on log2-transformed fold-changes and standard deviations[67]. Extra biochemical assays were usually used to validate the drug targets. ThermoTargetMiner, on the contrary, found out that fold-changes and p-values allow noise from irrelevant proteins to significantly fluctuate the determination of drug targets. Hereby, we introduced OPLS-DA followed by normalization to minimize the impact of such noise. In addition to that, we encourage cross-validating the targets between PISA datasets, meaning that no more experiments need to be conducted to validate a single protein target.

ThermoTargetMiner is a useful drug targets database. In our previous work ProTargetMiner, we demonstrated that FITExP is a useful assay to reveal protein targets based on drug-induced expression regulation[18]. Though the majority of approved drugs' well-defined targets are proteins[68], not all of these drugs work through regulating protein expression. For instance, kinase inhibitors are a large group of antineoplastic drugs that would inhibit the phosphorylation on signaling proteins. It is also well-known that small-molecule binding to protein can result in conformational changes[69]. PISA, as a supplementary assay for FITExP, is able to detect changes in protein solubility induced by modifications and structure alterations. In this work, we further developed PISA into a standard pipeline that is customized for large-scale drug screening. ThermoTargetMiner provides reliable data that includes novel targets for 67 FDA-approved anticancer compounds, enabling prediction and interpretation on side effects. The

bindings of small-molecule drugs to proteins that were never reported before could also inspire drug repurposing.

Conclusions

This study illustrates how higher-throughput PISA analysis can validate known targets, provide new target information, and help explain the mechanism of drug action. This approach offers a valuable framework for forecasting potential side effects and repurposing drugs for prospective indications. Last but not least, the wealth of target information provided in the ThermoTargetMiner resource holds broader implications beyond lung cancer, and can be extrapolated to various cancer types, to the benefit of a wider oncological community.

Methods

Selection of molecules

Clinical trial data for lung cancer were downloaded from https://clinicaltrials.gov/. Only compounds under clinical phase II and above were considered. The complete list of compounds is shown in **Table 1**. 14 compounds found in ProTargetMiner (crizotinib, docetaxel, ponatinib, sorafenib, sunitinib, gefitinib, lapatinib, pazopanib, ruxolitinib, apatinib, cabozantinib, fludarabine, topotecan and epirubicin)[18] were selected, along with 53 compounds chosen based on commercial availability and diversity of targets (at least one drug against each known target was included).

Selection of cell lines

A549 lung adenocarcinoma cells representing NSCLC and NCI-H82 [H82] cells representing SCLC were selected as model systems. A549 is a widely used lung cancer model system that was employed in at least 485,000 studies reported in Google Scholar, including ProTargetMiner[18]. NCI-H82 [H82] was chosen as a classic model of SCLC, because it is adherent and can be grown in the same medium (DMEM) as A549 cells. As this cell line is derived from a metastatic site, it is a good candidate for comparison of the results with A549 cells. None of these

cell lines are found in the Register of Misidentified Cell Lines (https://iclac.org/databases/cross-contaminations/).

Dose and duration of treatment

As compound screening assays for hit discovery are typically run at 1–10 μM[18], the same concentration of 10 μM was used for all the compounds. The incubation time in the lysate experiments was 30 min, while the cells were treated for 1 h to allow extra time for drug import or diffusion through the cell membrane.

Proteomics experimental design

In each experiment, two types of controls were used: cells treated with vehicle (DMSO) and with methotrexate (MTX). MTX targets the dihydrofolate reductase (DHFR) protein, which is readily identified in both PISA[12] and FITExP[19]. The assignment of each TMT channel to each treatment is shown in **Supplementary Table 1.**

PISA in lysate

PISA experiments were performed using the previously published method[12]. A549 and H82 cells were cultured in 175 cm^2 flasks, and were then detached, washed twice with PBS, and resuspended in PBS. The cell suspensions were freeze-thawed in liquid nitrogen 5 times, and then centrifuged at 10,000 g for 10 min to remove the cell debris. The protein concentration in the lysate was measured using Pierce BCA assay (Thermo). The cleared lysate was then aliquoted in 3 replicates and treated with the drugs for 30 min at 37°C in 300 μL reaction volume. After the reaction, the samples from each replicate were aliquoted into 10 wells in a 96-well plate and heated for 3 min in an Eppendorf gradient thermocycler (Eppendorf; Mastercycler X50s) in the temperature range of 48-59°C. Samples were then cooled for 3 min at room temperature (RT) and afterwards snap frozen and kept on ice. Samples from each replicate were then combined and transferred into polycarbonate thickwall tubes and centrifuged for 20 min at 100,000 g and 4°C.

The soluble protein fraction was transferred to new Eppendorf tubes. Protein concentration was measured in all samples using Pierce BCA Protein Assay Kit (Thermo), the volume corresponding to 25 μg of protein was transferred from each sample to new tubes and urea was added to a final concentration of 4 M. Dithiothreitol (DTT) was added to a final concentration of

10 mM and samples were incubated for 1 h at RT. Subsequently, iodoacetamide (IAA) was added to a final concentration of 50 mM and samples were incubated at RT for 1 h in the dark. The reaction was quenched by adding an additional 10 mM of DTT. No protein precipitation was performed, to avoid losing short semi-tryptic peptides at this stage. Lysyl endopeptidase (LysC; Wako) was added at a 1:75 w/w ratio and samples incubated at RT overnight. Samples were diluted with 20 mM EPPS to the final urea concentration of 1 M, and trypsin was added at a 1:75 w/w ratio, followed by incubation for 6 h at RT. Acetonitrile (ACN) was added to a final concentration of 20% and TMT reagents were added 4x by weight (200 µg) to each sample, followed by incubation for 2 h at RT. The reaction was quenched by addition of 0.5% hydroxylamine. Samples within each replicate were combined, acidified by TFA, cleaned using Sep-Pak cartridges (Waters) and dried using DNA 120 SpeedVac Concentrator (Thermo). The pooled samples were resuspended in 20 mM ammonium hydroxide and separated into 96 fractions on an XBrigde BEH C18 2.1x150 mm column (Waters; Cat#186003023), using a Dionex Ultimate 3000 2DLC system (Thermo Scientific) over a 48 min gradient of 1-63% B (B=20 mM ammonium hydroxide in acetonitrile) in three steps (1-23.5% B in 42 min, 23.5-54% B in 4 min and then 54-63% B in 2 min) at 200 µL min^{-1} flow. Fractions were then concatenated into 12 samples in sequential order (*e.g.*, fractions 1, 13, 25, …, and 85 were combined).

PISA in cells

Cells were cultured in 6-well plates to a density of 250,000 cells per plate. A day later, cells were treated with the drugs for 1 h. The cells were then washed with PBS, scraped off and resuspended in PBS. The cells were then aliquoted into 10 in PCR plates and heated like above. The cells were then snap-frozen and kept on ice. The samples from each replicate were then pooled and 0.4% final concentration of NP40 was added. The rest of the protocol was identical to PISA in lysate.

LC-MS/MS analysis and data acquisition

Orbitrap Fusion and Lumos mass spectrometers were used online with an Ultimate 3000 RSLC nanoUPLC system (Thermo Scientific). Sample fractions were dried and resuspended in Buffer A (0.1% FA and 2% acetonitrile in water) to a theoretical peptide concentration of 0.3 µg/µL. Resuspended peptides were loaded onto a Acclaim PepMap 100 C18 HPLC column (75 µm internal diameter, 3 µm beads, 100 Å pore size, Thermo, Cat#164535) for 5 min at a flow rate

of 4 μL/min. Peptides were transferred through an EASY-Spray column (75 μm internal diameter, 2 μm beads, 100 Å pore; Cat#ES903) connected to the Easy-Spray source (Thermo; Cat#ES082). Subsequently, the peptides were eluted with a buffer B (0.1% FA and 2% water in acetonitrile) gradient at a flow rate of 300 nL min^{-1}. The elution gradient was from 4% B to 28% B for 150 min, to 34% B for 15 min, increasing to 95% B in the next 3 min and staying at 95% for 4 min. Mass spectra were acquired with an Orbitrap Fusion Tribrid mass spectrometer (Thermo; Cat#IQLAAEGAAPFADBMBCX) in the data-dependent mode with MS1 analysis at 120,000, and MS2 at 50,000 resolution, in the m/z range from 400 to 1600. Peptide fragmentation was performed via higher-energy collision dissociation at 35% normalized collision energy.

Protein identification and data analysis

Raw LC-MS/MS data were processed for protein identification and quantification using MaxQuant software (2.5.0.0) with the UniProt human proteome database (UP000005640_9606 and UP000005640_9606_additional). No more than two missed cleavages were allowed. And the results were filtered to a 1% false discovery rate. Data post-processing was performed in R and OPLS-DA models were built using SIMCA 17 (Sartorius).

Statistics

Only proteins that were identified with two or more unique peptides and without potential contaminations were included in the final dataset. To calculate the fold-changes of the PISA signals, abundances of TMT reporters (peptide abundances) were first normalized to the total abundance in each TMT channel, followed by the protein abundances being calculated as the average of all normalized peptide abundances. Thereafter the protein abundances were normalized to those in the DMSO-treated samples (occupying the TMT126 channel in each TMT set, see Supplementary Table 1). The fold-changes were then calculated as the ratios of the protein abundances in treated samples vs those of the controls. Batch effects among three biological replicates were removed using Limma package[66]. For each protein, the median fold-change was used for further analysis, and the p-values were calculated by the two-sided Student's t-test on the normalized abundances in treated samples vs those in controls. In OPLS-DA analysis, protein coordinates were normalized first to the coordinates of the drug, and then to the standard deviation (SD) of the distribution of proteins' x-coordinates. The OPLS-DA-derived p-values were the GAUSS error function calculated for each protein based on its SD-normalized coordinate.

Data availability

The LC-MS/MS raw data files and extracted peptides and protein abundances are deposited in the PRIDE repository of the ProteomeXchange Consortium[70] under the dataset identifier PXD054158 with no restrictions. The source data underlying Supplementary Figures 1-71, and Supplementary Figures 74-145 are provided as a Source Data file. All other data are available from the corresponding authors on request.

Acknowledgements

This work was supported by Cancerfonden (grants 19 0558 Pj and 22 1967 Pj to RAZ). We would like to acknowledge Ákos Végvári and Xuepei Zhang for their assistance in LC-MS/MS analysis and Marie Ståhlberg and Carina Palmberg for their general assistance in lab work. We also appreciate Karolinska Institutet for open access funding. RAZ also acknowledges support from The Ministry of Science and Higher Education of RF (agreement № 075-15-2020-899), as well as RUDN project № 033322-2-000.

Author contributions

The concept, resources, experimental design, and methodology by R.A.Z., protocols and training by A.A.S.; sample preparation by H.L., A.A.S., B.S., A.V., and B.N.; LC-MS/MS analysis by H.L. and Z.M.; data analysis and visualization by H.L. and H.G.; writing - original draft by H.L. and R.A.Z., with editing by A.A.S. and reviewing by all other co-authors.

References

1. Thai, A. A., Solomon, B. J., Sequist, L. V., Gainor, J. F. & Heist, R. S. Lung cancer. *The Lancet* **398**, 535–554 (2021).

2. Zappa, C. & Mousa, S. A. Non-small cell lung cancer: Current treatment and future advances. *Transl Lung Cancer Res* (2016) doi:10.21037/tlcr.2016.06.07.

3. Rudin, C. M., Brambilla, E., Faivre-Finn, C. & Sage, J. Small-cell lung cancer. *Nat Rev Dis Primers* **7**, 3 (2021).

4. Duma, N., Santana-Davila, R. & Molina, J. R. Non–Small Cell Lung Cancer: Epidemiology, Screening, Diagnosis, and Treatment. *Mayo Clin Proc* **94**, 1623–1640 (2019).

5. Harrison, R. K. Phase II and phase III failures: 2013-2015. *Nat Rev Drug Discov* **15**, 817–818 (2016).

6. Sabatier, P., Beusch, C. M., Meng, Z. & Zubarev, R. A. System-Wide Profiling by Proteome Integral Solubility Alteration Assay of Drug Residence Times for Target Characterization. *Anal Chem* **94**, 15772–15780 (2022).

7. Sun, D., Gao, W., Hu, H. & Zhou, S. Why 90% of clinical drug development fails and how to improve it? *Acta Pharm Sin B* **12**, 3049–3062 (2022).

8. Lin, A. *et al.* Off-target toxicity is a common mechanism of action of cancer drugs undergoing clinical trials. *Sci Transl Med* **11**, (2019).

9. Vedadi, M. *et al.* Chemical screening methods to identify ligands that promote protein stability, protein crystallization, and structure determination. *Proc Natl Acad Sci U S A* **103**, 15835–15840 (2006).

10. Molina, D. M. *et al.* Monitoring drug target engagement in cells and tissues using the cellular thermal shift assay. *Science (1979)* **341**, 84–87 (2013).

11. Savitski, M. M. *et al.* Tracking cancer drugs in living cells by thermal profiling of the proteome. *Science (1979)* (2014) doi:10.1126/science.1255784.

12. Gaetani, M. *et al.* Proteome Integral Solubility Alteration: A High-Throughput Proteomics Assay for Target Deconvolution. *J Proteome Res* **18**, 4027–4037 (2019).

13. Zhang, X. *et al.* Solvent-Induced Protein Precipitation for Drug Target Discovery on the Proteomic Scale. *Anal Chem* **92**, 1363–1371 (2020).

14. Beusch, C. M., Sabatier, P. & Zubarev, R. A. Ion-Based Proteome-Integrated Solubility Alteration Assays for Systemwide Profiling of Protein−Molecule Interactions. *Anal Chem* **94**, 7066–7074 (2022).

15. Saei, A. A. *et al.* System-wide identification and prioritization of enzyme substrates by thermal analysis. *Nat Commun* **12**, 1–13 (2021).

16. Saei, A. A. *et al.* Massive Solubility Changes in Neuronal Proteins upon Simulated Traumatic Brain Injury Reveal the Role of Shockwaves in Irreversible Damage. *Molecules* **28**, 6768 (2023).

17. Saei, A. A. *et al.* Mapping the GALNT1 substrate landscape with versatile proteomics tools. *bioRxiv* 2022.08.24.505189 (2022) doi:10.1101/2022.08.24.505189.

18. Saei, A. A. *et al.* ProTargetMiner as a proteome signature library of anticancer molecules for functional discovery. *Nat Commun* (2019) doi:10.1038/s41467-019-13582-8.

19. Chernobrovkin, A., Marin-Vicente, C., Visa, N. & Zubarev, R. A. Functional Identification of Target by Expression Proteomics (FITExP) reveals protein targets and highlights mechanisms of action of small molecule drugs. *Scientific Reports 2015 5:1* **5**, 1–9 (2015).

20. Zhang, S. *et al.* The potent ALK inhibitor brigatinib (AP26113) overcomes mechanisms of resistance to first- and second-generation ALK inhibitors in preclinical models. *Clinical Cancer Research* **22**, 5527–5538 (2016).

21. Gerber, D. E. *et al.* Phase 2 study of the focal adhesion kinase inhibitor defactinib (VS-6063) in previously treated advanced KRAS mutant non-small cell lung cancer. *Lung Cancer* **139**, 60–67 (2020).

22. Wolenski, F. S. *et al.* The NAE inhibitor pevonedistat (MLN4924) synergizes with TNF-α to activate apoptosis. *Cell Death Discovery 2015 1:1* **1**, 1–9 (2015).

23. Szklarczyk, D. *et al.* The STRING database in 2023: protein-protein association networks and functional enrichment analyses for any sequenced genome of interest. *Nucleic Acids Res* **51**, D638–D646 (2023).

24. Shimamura, T. *et al.* Ganetespib (STA-9090), a Non-Geldanamycin HSP90 Inhibitor, has Potent Antitumor Activity in In Vitro and In Vivo Models of Non-Small Cell Lung Cancer. *Clin Cancer Res* **18**, 4973 (2012).

25. Wishart, D. S. *et al.* DrugBank: a knowledgebase for drugs, drug actions and drug targets. *Nucleic Acids Res* **36**, (2008).

26. Rajagopalan, P. T. R. *et al.* Interaction of dihydrofolate reductase with methotrexate: Ensemble and single-molecule kinetics. *Proc Natl Acad Sci U S A* **99**, 13481 (2002).

27. Mendel, D. B. *et al.* In Vivo Antitumor Activity of SU11248, a Novel Tyrosine Kinase Inhibitor Targeting Vascular Endothelial Growth Factor and Platelet-derived Growth Factor Receptors: Determination of a Pharmacokinetic/Pharmacodynamic Relationship.

28. Beauchamp, E. *et al.* Targeting N-myristoylation for therapy of B-cell lymphomas. *Nature Communications 2020 11:1* **11**, 1–16 (2020).

29. Mooney, L., Skinner, M., Coker, S. J. & Currie, S. Effects of acute and chronic sunitinib treatment on cardiac function and calcium/calmodulin-dependent protein kinase II. *Br J Pharmacol* **172**, 4342 (2015).

30. Modi, V. & Dunbrack, R. L. Defining a new nomenclature for the structures of active and inactive kinases. *Proc Natl Acad Sci U S A* **116**, 6818–6827 (2019).

31. Karaman, M. W. *et al.* A quantitative analysis of kinase inhibitor selectivity. *Nature Biotechnology 2008 26:1* **26**, 127–132 (2008).

32. Wang, X., Zhang, Y., Han, Z. G. & He, K. Y. Malignancy of Cancers and Synthetic Lethal Interactions Associated With Mutations of Cancer Driver Genes. *Medicine* **95**, (2016).

33. Anastassiadis, T., Deacon, S. W., Devarajan, K., Ma, H. & Peterson, J. R. Comprehensive assay of kinase catalytic activity reveals features of kinase inhibitor selectivity. *Nat Biotechnol* **29**, 1039–1045 (2011).

34. Gupta, P., Wright, S. E., Kim, S. H. & Srivastava, S. K. Phenethyl Isothiocyanate: A comprehensive review of anti-cancer mechanisms. *Biochim Biophys Acta* **1846**, 405 (2014).

35. Mi, L. *et al.* Covalent Binding to Tubulin by Isothiocyanates: A MECHANISM OF CELL GROWTH ARREST AND APOPTOSIS*S. *J Biol Chem* **283**, 22136 (2008).

36. Nilsson, R. *et al.* Metabolic enzyme expression highlights a key role for MTHFD2 and the mitochondrial folate pathway in cancer. *Nature Communications 2014 5:1* **5**, 1–10 (2014).

37. Edvardson, S. *et al.* Infantile neurodegenerative disorder associated with mutations in TBCD, an essential gene in the tubulin heterodimer assembly pathway. *Hum Mol Genet* **25**, 4635–4648 (2016).

38. Goodin, S., Kane, M. P. & Rubin, E. H. Epothilones: Mechanism of action and biologic activity. *Journal of Clinical Oncology* **22**, 2015–2025 (2004).

39. WO2017023866 METHOD OF TARGETING STAT3 AND OTHER NON-DRUGGABLE PROTEINS. https://patentscope.wipo.int/search/en/detail.jsf?docId=WO2017023866.

40. Holmgren, A. Thioredoxin and Glutaredoxin Systems. *Journal of Biological Chemistry* **264**, 13963–13966 (1989).

41. Froeling, F. E. M. *et al.* Bioactivation of napabucasin triggers reactive oxygen species–mediated cancer cell death. *Clin Cancer Res* **25**, 7162 (2019).

42. Jin, H. *et al.* Systematic transcriptional analysis of human cell lines for gene expression landscape and tumor representation. *Nat Commun* **14**, (2023).

43. Cell line - NQO1 - The Human Protein Atlas. https://www.proteinatlas.org/ENSG00000181019-

NQO1/cell+line#lung_cancerhttps://www.proteinatlas.org/ENSG00000181019-NQO1/cell+line#lung_cancer.

44. Klaeger, S. *et al.* The target landscape of clinical kinase drugs. *Science* **358**, (2017).

45. Ren, B. J. *et al.* Alisertib Induces Cell Cycle Arrest, Apoptosis, Autophagy and Suppresses EMT in HT29 and Caco-2 Cells. *Int J Mol Sci* **17**, (2016).

46. Kläger, S. E. Chemical Proteomics Reveals the Target Landscape of Clinical Kinase Inhibitors.

47. Peng, K. *et al.* Development of combination strategies for Focal Adhesion Kinase inhibition in Diffuse Gastric Cancer. *Clin Cancer Res* **29**, 197 (2023).

48. Ardini, E. *et al.* Entrectinib, a Pan-TRK, ROS1, and ALK inhibitor with activity in multiple molecularly defined cancer indications. *Mol Cancer Ther* **15**, 628–639 (2016).

49. Witzig, T. E. *et al.* The mTORC1 inhibitor everolimus has antitumor activity in vitro and produces tumor responses in patients with relapsed T-cell lymphoma. *Blood* **126**, 328–335 (2015).

50. Hansen, N. T., Brunak, S. & Altman, R. B. Generating Genome-Scale Candidate Gene Lists for Pharmacogenomics. *Clin Pharmacol Ther* **86**, 183 (2009).

51. Dhillon, S. Lonafarnib: First Approval. *Drugs* **81**, 283 (2021).

52. Rajagopalan, P. T. R. *et al.* Interaction of dihydrofolate reductase with methotrexate: Ensemble and single-molecule kinetics. *Proc Natl Acad Sci U S A* **99**, 13481 (2002).

53. Uga, H. *et al.* A New Mechanism of Methotrexate Action Revealed by Target Screening with Affinity Beads. *Mol Pharmacol* **70**, 1832–1839 (2006).

54. Cao, X. *et al.* ROS-mediated hypomethylation of PRDX5 promotes STAT3 binding and activates the Nrf2 signaling pathway in NSCLC. *Int J Mol Med* **47**, 573 (2021).

55. Froeling, F. E. M. *et al.* Bioactivation of Napabucasin Triggers Reactive Oxygen Species-Mediated Cancer Cell Death. *Clin Cancer Res* **25**, 7162–7174 (2019).

56. Marchetti, C. *et al.* Olaparib, PARP1 inhibitor in ovarian cancer. *Expert Opin Investig Drugs* **21**, 1575–1584 (2012).

57. Braal, C. L. *et al.* Inhibiting CDK4/6 in Breast Cancer with Palbociclib, Ribociclib, and Abemaciclib: Similarities and Differences. *Drugs* **81**, 317 (2021).

58. Czuczman, N. M. *et al.* Pevonedistat, a NEDD8-activating enzyme inhibitor, is active in mantle cell lymphoma and enhances rituximab activity in vivo. *Blood* **127**, 1128 (2016).

59. Mi, L. *et al.* Covalent Binding to Tubulin by Isothiocyanates: A MECHANISM OF CELL GROWTH ARREST AND APOPTOSIS*S. *J Biol Chem* **283**, 22136 (2008).

60. Upadhyaya, B., Liu, Y. & Dey, M. Phenethyl Isothiocyanate Exposure Promotes Oxidative Stress and Suppresses Sp1 Transcription Factor in Cancer Stem Cells. *Int J Mol Sci* **20**, (2019).

61. Sarker, D. *et al.* First-in-human Phase I study of Pictilisib (GDC-0941), a potent pan-class I phosphatidylinositol-3-kinase (PI3K) inhibitor, in patients with advanced solid tumors. *Clin Cancer Res* **21**, 77 (2015).

62. Hnatiuk, A. P. *et al.* Reengineering Ponatinib to Minimize Cardiovascular Toxicity. *Cancer Res* **82**, 2777 (2022).

63. Liu, C. *et al.* Ponatinib Inhibits Proliferation and Induces Apoptosis of Liver Cancer Cells, but Its Efficacy Is Compromised by Its Activation on PDK1/Akt/mTOR Signaling. *Molecules* **24**, (2019).

64. Lugowska, I., Koseła-Paterczyk, H., Kozak, K. & Rutkowski, P. Trametinib: a MEK inhibitor for management of metastatic melanoma. *Onco Targets Ther* **8**, 2251 (2015).

65. Richon, V. M. Cancer biology: mechanism of antitumour action of vorinostat (suberoylanilide hydroxamic acid), a novel histone deacetylase inhibitor. *British Journal of Cancer 2006 95:1* **95**, S2–S6 (2006).

66. Batth, T. S. *et al.* STREAMLINED PROTEOME-WIDE IDENTIFICATION OF DRUG TARGETS INDICATES ORGAN-SPECIFIC ENGAGEMENT. *bioRxiv* 2024.02.08.578880 (2024) doi:10.1101/2024.02.08.578880.

67. Vranken, J. G. Van *et al.* Large-scale characterization of drug mechanism of action using proteome-wide thermal shift assays. *bioRxiv* (2024) doi:10.1101/2024.01.26.577428.

68. Eder, J., Sedrani, R. & Wiesmann, C. The discovery of first-in-class drugs: origins and evolution. *Nature Reviews Drug Discovery 2014 13:8* **13**, 577–587 (2014).

69. Ayaz, P. *et al.* Structural mechanism of a drug-binding process involving a large conformational change of the protein target. *Nature Communications 2023 14:1* **14**, 1–15 (2023).

70. Vizcaíno, J. A. *et al.* ProteomeXchange provides globally coordinated proteomics data submission and dissemination. *Nature Biotechnology* Preprint at https://doi.org/10.1038/nbt.2839 (2014).